

Transcriptional Regulation, Metal Binding Properties and Structure of Pden1597, an Unusual Zinc Transport Protein from *Paracoccus denitrificans**

Received for publication, February 13, 2015, and in revised form, March 16, 2015 Published, JBC Papers in Press, March 18, 2015, DOI 10.1074/jbc.M115.645853

Melody Handali, Durga P. Neupane, Hridindu Roychowdhury, and Erik T. Yukl¹

From the Department of Chemistry and Biochemistry, New Mexico State University, Las Cruces, New Mexico 88003

Background: Bacterial cluster 9 ATP binding cassette (ABC) transporters are responsible for import of Zn^{2+} and Mn^{2+} .

Results: A solute-binding protein of the cluster 9 family is shown to preferentially bind Zn^{2+} in an unusual coordination sphere.

Conclusion: A subclass of Zn^{2+} transporter has been identified with distinct structural properties.

Significance: Cluster 9 ABC transporters are important virulence factors.

ATP-binding cassette (ABC) transporters of the cluster 9 family are ubiquitous among bacteria and essential for acquiring Zn^{2+} and Mn^{2+} from the environment or, in the case of pathogens, from the host. These rely on a substrate-binding protein (SBP) to coordinate the relevant metal with high affinity and specificity and subsequently release it to a membrane permease for translocation into the cytoplasm. Although a number of cluster 9 SBP structures have been determined, the structural attributes conferring Zn^{2+} or Mn^{2+} specificity remain ambiguous. Here we describe the gene expression profile, *in vitro* metal binding properties, and crystal structure of a new cluster 9 SBP from *Paracoccus denitrificans* we have called AztC. Although all of our results strongly indicate Zn^{2+} over Mn^{2+} specificity, the Zn^{2+} ion is coordinated by a conserved Asp residue only observed to date as a metal ligand in Mn^{2+} -specific SBPs. The unusual sequence properties of this protein are shared among close homologues, including members from the human pathogens *Klebsiella pneumonia* and *Enterobacter aerogenes*, and would seem to suggest a subclass of Zn^{2+} -specific transporters among the cluster 9 family. In any case, the unusual coordination environment of AztC expands the already considerable range of those available to Zn^{2+} -specific SBPs and highlights the presence of a His-rich loop as the most reliable indicator of Zn^{2+} specificity.

The transition metals Mn^{2+} , Fe^{2+} , Cu^{2+} , and Zn^{2+} are required for a tremendous number of essential cellular processes (1), making their efficient acquisition a prerequisite for life. Therefore, all organisms have adapted systems to import these metals across the cell membrane, as well as efflux systems to prevent metal toxicity. High affinity import systems are particularly important for bacteria colonizing environments that are strictly limited in essential metals. Pathogenic bacteria face such conditions within the human host where levels of “free”

Fe^{2+} , Mn^{2+} , and Zn^{2+} are severely limited (2). As a consequence, high affinity transporter systems for these metals have been identified as important virulence factors (3). One important class of these, the ATP binding cassette (ABC)² transporters, are composed of a membrane spanning permease, a cytoplasmic ATPase, and a solute-binding protein (SBP). In Gram-negative bacteria, SBPs are soluble, periplasmic proteins, whereas Gram-positive species utilize lipoprotein SBPs. In either case, the SBP confers high affinity and specificity to the system by binding the relevant metal and delivering it to the permease for translocation into the cytoplasm.

Phylogenetic analysis of SBPs revealed that they segregate into 8 clusters based on sequence homology and solute specificity (4). A ninth cluster was later proposed (5), which subdivided into two groups apparently specific for $\text{Zn}(\text{II})$ or $\text{Mn}(\text{II})$ (6). Representatives of the so-called cluster 9 (also known as cluster A-I) ABC transporters are critical for virulence in various pathogens including *Salmonella enterica* (7), *Yersinia pestis* (8), *Streptococcus pneumonia* (9), and *Bacillus anthracis* (10) among others. This appears to be largely due to severe limitation of free Mn^{2+} and Zn^{2+} within the animal host mediated by sequestration of these metals by the host protein calprotectin (11–13). Thus, there is significant interest in the cluster 9 ABC transporters as potential targets for novel antibiotics.

Regarding metal specificity, it has been observed that many of the confirmed Zn^{2+} -specific SBPs contain a highly charged and His-rich loop (Fig. 1) proposed to facilitate Zn^{2+} acquisition (14). Although such sequences seem to be absent from Mn^{2+} transporters, the length of this feature in putative Zn^{2+} transporters is highly variable, potentially making this an imperfect indicator of metal specificity. Similarly, no clear picture emerges from the coordination environments of structurally characterized cluster 9 SBPs. The Zn^{2+} -specific SBP structures show coordination of Zn^{2+} through 3 His residues and 1 Glu or a water molecule (14–19), whereas the Mn^{2+} -specific SBPs prefer a harder coordination sphere of 2 Asp/Glu and 2

* This work was supported, in whole or in part, by National Institutes of Health Grant SC2 GM111170-01 from the NIGMS.

The atomic coordinates and structure factors (code 4XRV) have been deposited in the Protein Data Bank (<http://www.pdb.org/>).

¹ To whom correspondence should be addressed: 1175 N. Horseshoe Dr., Las Cruces, NM 88003. Tel.: 575-646-3176; Fax: 575-646-2649; E-mail: etyukl@nmsu.edu.

² The abbreviations used are: ABC, ATP binding cassette; SBP, solute-binding protein; TPEN, *N,N,N',N'*-tetrakis(2-pyridylmethyl)ethane-1,2-diamine; qRT, quantitative real time; ICP-OES, inductively coupled plasma-optical emission spectroscopy; MF-2, mag-fura-2; Bistris propane, 1,3-bis[tris(hydroxymethyl)methylamino]propane.

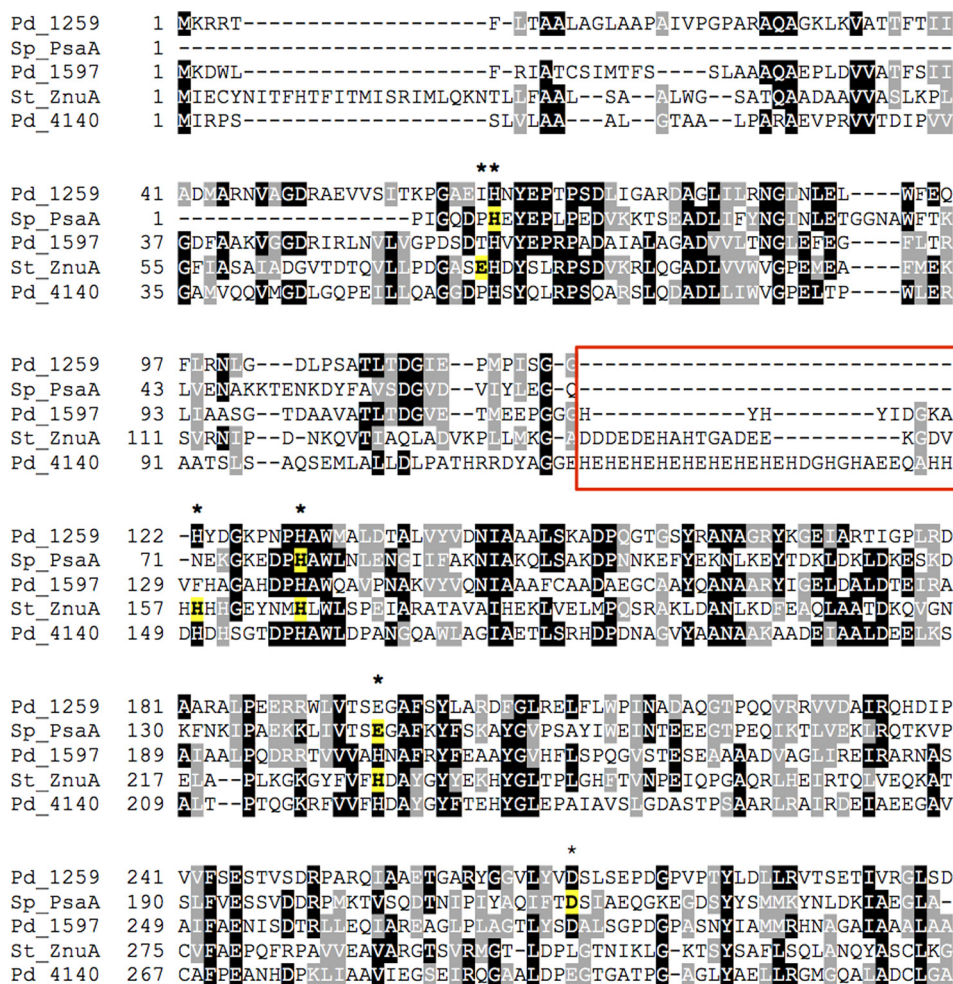


FIGURE 1. Multiple sequence alignments of Pden1597 with putative Mn^{2+} (Pden1259) and Zn^{2+} (Pden4140) SBPs from *P. denitrificans*, the Mn^{2+} SBP PsaA from *Streptococcus pneumoniae* (Sp_PsaA) and the Zn^{2+} SBP ZnuA from *Salmonella typhimurium* (St_ZnuA). Black and gray shading indicate regions of sequence identity and similarity, respectively. Asterisks above the sequences indicate possible positions of metal ligands, whereas residues highlighted in yellow are metal ligands observed in crystal structures. The red box highlights the His-rich loop observed in Zn-specific SBPs.

His (20–26), with the exception of TroA, which uses only 1 Asp and 3 His residues (27–29). Further complicating the situation is the observation that some of the SBPs are not crystallized with their cognate metal, or the identity of the physiologically relevant metal has not been determined by independent means.

Based on a simple BLAST search, the genome of *Paracoccus denitrificans* contains 3 ABC transporters of the cluster 9 family (Fig. 1) identified by SBP genes *pden1259*, *pden1597*, and *pden4140*. *Pden1259* is homologous to the Mn^{2+} SBP MtsA from *S. pneumoniae* (31.6% sequence identity) including the absolute conservation of metal ligands and the absence of a His-rich sequence. Similarly, *pden4140* is homologous to the Zn^{2+} SBP ZnuA from *S. enterica* (28.7% sequence identity) including absolute conservation of metal ligands and the presence of a particularly large His-rich region. The final gene, *pden1597*, falls somewhere in between, with slightly higher homology to SpMtsA than StZnuA (26.4 versus 20.2%, respectively) and a severely abbreviated His-rich sequence. Similarly, the presence of a His at position 204 suggests Zn^{2+} specificity, whereas an Asp at position 279 suggests Mn^{2+} specificity. Thus, *P. denitrificans* Pden1597 presents an excellent opportu-

nity to test the determinants of metal ion specificity among the cluster 9 family of ABC transporters.

Here we have analyzed expression of the above genes under Zn^{2+} - and Mn^{2+} -limiting conditions as well as the *in vitro* metal binding properties and structure of Pden1597. The expression of *pden1597* is increased under conditions of Zn^{2+} starvation but not during Mn^{2+} starvation, and heterologously expressed Pden1597 binds Zn^{2+} with an affinity ~ 100 -fold greater than that for Mn^{2+} . Unexpectedly, the structure of Pden1597 shows that Zn^{2+} is coordinated by Asp-279, which has never been observed for a Zn^{2+} -specific SBP. Based on these results, we propose that Pden1597 is a Zn^{2+} -specific transporter with an unusual metal binding site. These experiments expand the range of flexibility available to the cluster 9 SBPs in regard to metal coordination and highlight the presence of a His-rich sequence as the most reliable indication of Zn^{2+} specificity within this family.

EXPERIMENTAL PROCEDURES

Bacterial Growth Conditions and Harvesting of Cells—A minimal media composition using an organic phosphate source

An unusual Zn^{2+} -specific Solute-binding Protein

and succinate as a carbon source was developed based on Graham *et al.* (30) and Wang *et al.* (31). Bulk media containing 40 mM MES, 20 mM KCl, 60 mM NH_4Cl , and 0.5 g/liter of yeast extract at pH 7.4 was passed through a Chelex (Bio-Rad) column into an acid-washed bottle to minimize contaminating metal ions. The solution was then supplemented with 134 μM EDTA, 250 μM CaCl_2 , 810 μM MgSO_4 before autoclaving. Succinate at 1.0 M and 764 mM β -phosphoglycerate were prepared separately, passed through Chelex into acid-washed bottles, and autoclaved. Concentrated metal salt solutions of 50 mM ZnSO_4 , 47 mM MnSO_4 , 53 mM NaMoO_4 , 1.6 mM CuCl_2 , and 20 mM Fe^{2+} -citrate (5.5 g/liter of $\text{FeSO}_4 \cdot 7\text{H}_2\text{O}$ and 5.35 g/liter of citric acid) were also prepared separately and filter sterilized. Replete media was made by combining the above components to final concentrations of 38 mM MES, 19 mM KCl, 57 mM NH_4Cl , 0.47 g/liter of yeast extract, 126 μM EDTA, 236 μM CaCl_2 , 764 μM MgSO_4 , 50 mM succinate, 7.6 mM β -phosphoglycerate, 50 μM ZnSO_4 , 47 μM MnSO_4 , 53 μM NaMoO_4 , 1.6 μM CuCl_2 , and 20 μM Fe^{2+} -citrate. Zn^{2+} -depleted and Mn-depleted media were made by the omission of ZnSO_4 and MnSO_4 , respectively. Zn^{2+} -chelated medium was made by the addition of *N,N,N',N'*-tetrakis(2-pyridylmethyl)ethane-1,2-diamine (TPEN) to Zn^{2+} -depleted media to a final concentration of 50 μM .

An overnight culture of *P. denitrificans* PD1222 cells grown in replete media was used to inoculate three replicates of each of the four different media types described above. The growth of cells in all four conditions was monitored at 600 nm using an Agilent Cary 60 UV-visible spectrophotometer and 5 ml of cells at midexponential phase ($A_{600\text{ nm}}$ 0.4–0.6) were harvested from each condition. To preserve RNA, 2 ml of ice-cold 5% (v/v) phenol in ethanol were added and incubated on ice for 30 min prior to centrifugation and storage at -80°C until RNA was isolated.

RNA Extraction and qRT-PCR—RNA was extracted and purified from the replicate samples described above using a PureLink[®] RNA Mini Kit (Ambion) according to the manufacturer's instructions. Contaminating DNA was removed by an on-column DNase digestion protocol (Invitrogen). RNA concentration and purity were determined spectrophotometrically using a Nanodrop Spectrophotometer (ND 1000).

Purified RNA (1 μg) was reverse transcribed to cDNA using iScript[™] cDNA synthesis kit (Bio-Rad) according to the manufacturer's instructions. cDNA was diluted 5-fold in H_2O before use in qPCR. Primers were designed to amplify 100–150 bp regions of each gene with a T_m $\sim 60^\circ\text{C}$ and used at a final concentration of 0.3 μM . Quantitative real-time PCR was done using Power SYBR[®] Green PCR Master Mix (Applied Biosystems) and a CFX96 RT-PCR real-time system combined with a C1000 Thermal cycler (Bio-Rad). Relative transcript abundance was normalized to *dnan*, encoding the β -subunit of DNA-polymerase III (Pden_0970), a housekeeping gene previously used for *P. denitrificans* RT-PCR experiments (32).

Cloning, Heterologous Expression, and Purification—The entire *pden1597* gene was amplified by PCR from genomic DNA using the following primers: 5'-GCTGTCCATGGCAA-TGAAAGACTGGCTCTTCCGC-3' forward and 5'-ACTATGGATCCTCAGCGGGCGGCCAGCGC-3' reverse. The PCR product was cloned into a pET-45(b)⁺ vector (Novagen) using

NcoI and BamHI restriction sites, resulting in a translated protein lacking any affinity tags and containing the N-terminal periplasmic targeting sequence. Plasmid was transformed into BL21(DE3) *Escherichia coli* cells, which were grown in LB medium containing 100 $\mu\text{g}/\text{ml}$ of ampicillin at 37°C and 250 rpm to an $A_{600} = 0.8$ –1.0. Overexpression was then induced by addition of isopropyl 1-thio- β -D-galactopyranoside to 1.0 mM, the temperature was decreased to 20°C , and the cells were grown with shaking overnight. Cells were harvested by centrifuging at $3000 \times g$ for 30 min at 4°C .

The periplasmic fraction was obtained using an osmotic shock protocol adapted from Wang *et al.* (31). Briefly, the cell pellet was resuspended at 5 ml/g of wet weight cells in 50 mM phosphate, pH 8, 0.5 M sucrose, 0.67 mM EDTA, and 7.5 mg/ml of lysozyme and incubated at 30°C for 15 min. An equal volume of deionized water was added and incubated a further 45 min at 30°C . NaCl and MgCl_2 were then added to 300 and 0.5 mM, respectively. Cell debris was removed by centrifugation at $25,000 \times g$ for 30 min at 4°C , leaving the periplasmic fraction in the supernatant. Polyethyleneimine was added to 0.5% (v/v) to precipitate nucleic acids, which were removed by centrifugation at $25,000 \times g$ for 30 min at 4°C . Finally, the protein was precipitated by addition of ammonium sulfate to 60% (w/v) and centrifuged as above.

The ammonium sulfate pellet was dissolved in 20 mM Tris, pH 8.0, and centrifuged at $20,000 \times g$ at 4°C for 30 min to remove any remaining particulates. The supernatant was loaded onto a HiTrap Q HP column (GE Healthcare) equilibrated with 20 mM Tris, pH 8.0. The NaCl concentration was stepped to 150 mM NaCl and a linear gradient of NaCl applied to 350 mM NaCl. The peak containing Pden1597 eluted at ~ 250 mM NaCl. Fractions containing Pden1597 were combined and concentrated to 500 μl , and applied to a HiPrep Sephacryl S-100 HR column (GE Healthcare) equilibrated with 20 mM Tris, pH 8.0, 150 mM NaCl, 0.1 mM DTT. At this point, the protein was highly pure as judged by SDS-PAGE. Protein concentration was determined using an extinction coefficient at 280 nm of $19,691\text{ M}^{-1}\text{ cm}^{-1}$ calculated as previously described (33).

In-gel Trypsin Digests and Mass Spectrometry—In SDS-PAGE gels of Pden1597 purification fractions, the band corresponding to Pden1597 in the periplasmic fraction was excised and subjected to in-gel proteolysis (34) using trypsin (New England Biolabs). Extracted peptides were then evaporated to dryness, reconstituted in 0.1% (v/v) formic acid, and desalted/exchanged into 75:25 (v/v) acetonitrile/water with 0.1% (v/v) formic acid using C18 resin ZipTip pipette tips (Millipore) prior to introduction into the mass spectrometer. Peptide solutions were analyzed by direct-infusion electrospray ionization Fourier transform-ion cyclotron resonance mass spectrometry (Thermo LTQ FT) in positive ion mode. Nanoelectrospray was performed with an Advion NanoMate and the resulting peptide ions were measured in a parent-ion Fourier transform-ion cyclotron resonance scan at a resolving power of $m/\Delta m_{50\%} = 100,000$ at m/z 400. Fragment ion spectra were generated in the linear ion trap with peak picking based on the Fourier transform-ion cyclotron resonance spectrum and dynamic elution enabled. Parent ion and MS/MS data were manually inspected

using Xcalibur software version 2.1.0 to identify and confirm peptides of interest.

Metal Content Analysis—Protein samples at a concentration of 10–20 μM were digested in 4 M HNO_3 overnight at 70 °C to ensure their complete degradation. Prior to metal analysis, samples were diluted 2.5-fold with MilliQ water. For depleted media samples, 2.5 ml were combined with 0.5 ml of concentrated HNO_3 and digested overnight at 70 °C. Samples were analyzed on a Perkin-Elmer 2100 DV inductively coupled plasma-optical emission spectrometer (ICP-OES), calibrated with a multielement standard (Ricca Chemical). The wavelengths for measuring Mn^{2+} and Zn^{2+} were 257.610 and 206.200 nm, respectively, and samples were run in triplicate.

Generation of Apo-proteins—Apo-Pden1597 was generated by dialyzing the isolated protein against two changes of 500 ml of 50 mM NaOAc buffer, pH 4.5, 50 mM EDTA, and 150 mM NaCl. This was followed by a final dialysis against 500 ml of 20 mM Tris buffer, pH 8.0, 150 mM NaCl, and 3.4 g/liter of Chelex. The structural integrity of the protein was determined by the use of size exclusion chromatography, where it ran as a single peak consistent with its intact, monomeric molecular weight. Metal content was assessed by ICP-OES.

Metal Binding Affinity—All of the metal binding affinity experiments were performed in a 20 mM HEPES, pH 7.2, 200 mM NaCl, and 5% (v/v) glycerol buffer. This buffer was run through a Chelex column to remove any divalent metal ion contaminants. The fluorescent dye mag-fura-2 (MF-2) (Invitrogen) was used to analyze the metal binding affinities of apo-Pden1597 for Mn^{2+} and Zn^{2+} as previously described (35). All fluorescence measurements were made using a Varian Cary Eclipse fluorescence spectrophotometer with entrance and exit slits set to 10 nm. The protein concentration was measured before each experiment and the MF-2 concentration was determined using an extinction coefficient at 369 nm of $22,000 \text{ M}^{-1} \text{ cm}^{-1}$ (35). In each experiment, 1.0–15.0 μM apo-Pden1597 and 0.4–0.8 μM MF-2 were titrated with increasing concentrations of MnCl_2 or ZnSO_4 , keeping the total volume of titrant added to less than 10% (v/v). Pden1597 as isolated with stoichiometric Zn^{2+} was used at 15.0 μM and titrated with MnCl_2 in the presence of MF-2 to assess whether Mn^{2+} and Zn^{2+} bind to the same site. Fluorescence excitation spectra were scanned from 250 to 450 nm while monitoring emission at 505 nm. Experiments were performed in triplicate and the fluorescence intensities at $\lambda_{\text{ex}} = 330 \text{ nm}$ (Zn^{2+}) or 360 nm (Mn^{2+}) were fit using the program DYNAFIT (36, 37) using scripts adapted from Golynskiy *et al.* (35). An example of a script used for fitting Mn^{2+} binding is shown in Scheme 1.

Circular Dichroism—Circular dichroism (CD) spectra were recorded at 25 °C using a Jasco-810 spectropolarimeter with a cuvette chamber regulated by a PTC-4235 Peltier device (Jasco). Apo-Pden1597 was diluted to 15 μM in 5 mM HK_2PO_4 , pH 8.0, 150 mM NaCl in a 1-mm quartz cuvette. Where appropriate, ZnSO_4 or MnCl_2 were added to 40 μM . Spectra were acquired from 190 to 260 nm at 1 nm bandwidth, 2-s response time, 0.5 nm data pitch, and 10 nm/min scan speed. Each spectrum is the average of three accumulations and has been converted to mean residue ellipticity. For thermal stability experiments, the wavelength at 223 nm was monitored from 25 to

```
[task]
task = fit
data = equilibria

[mechanism]
M + MF2 <=> MMF2 : Kd1  dissoc
M + Pd97 <=> MPd97 : Kd2  dissoc

[constants]
Kd1 = 0.97
Kd2 = 0.05 ?

[responses]
MF2 = 0
MMF2 = 706 ?

[concentrations]
MF2 = 0.86
Pd97 = 0.5 ?

[data]
variable  M
set        substr

offset      0

[output]
directory ./examples
;
```

[set:substr]

| $M, \mu\text{M}$ | Int (unit) |
|------------------|------------|
| 0 | 0 |
| 0.015 | 6.109 |
| 0.163 | 9.37 |
| 0.456 | 18.58 |
| 0.743 | 102.23 |
| 1.024 | 167.54 |
| 1.311 | 224.57 |
| 2.027 | 315.46 |
| 3.448 | 429.54 |
| 6.250 | 496.12 |
| 20.32 | 561.01 |

[end]

SCHEME 1

90 °C every 0.2 °C with a constant heating rate of 1.0 °C/min. The fraction of folded protein at a given temperature T was determined using the following equation (38).

$$\text{Fraction Folded} = \frac{\theta_T - \theta_{75}}{\theta_{55} - \theta_{75}} \quad (\text{Eq. 1})$$

For the apo-protein, values of θ at 55 and 75 °C were deemed to correspond to 100 and 0% folded state, respectively. After thermal denaturation experiments, the spectra from 190 to 260 nm were again collected after returning to 25 °C to determine reversibility.

Crystallization and Structure Determination—Initial crystallization hits were identified using the Haupton Woodward Institute standard screen (39). These were optimized in house and diffraction quality crystals were grown under paraffin oil using a 1:1 ratio of 25 mg/ml of Pden1597 and precipitant solution containing 3.9 M sodium formate and 0.1 M bis-tris propane, pH 7.0, at 292 K. Crystals were cryoprotected with a 1:1

An unusual Zn^{2+} -specific Solute-binding Protein

mixture of paratone/paraffin prior to cryocooling in liquid nitrogen.

Diffraction data were collected at 100 K on beamline 5.0.2 at the Advanced Light Source at Berkeley National Laboratory, indexed and integrated with iMosfilm (40) and scaled using Aimless (41). A polyalanine model of MtsA (PDB code 3HH8) (26) was used as the search model for molecular replacement using Phaser-MR (42). The initial solution was subjected to several rounds of automated model building, density modification, and refinement using the AutoBuild Wizard in Phenix (43). Manual model building was done in Coot (44) and further rounds of refinement were done in REFMAC (45).

Pden1597 crystallized in space group C2 with two copies of the protein in the asymmetric unit. Near the end of refinement, a single Zn^{2+} was modeled at full occupancy bound to each protein molecule, and flexible bond restraints between Zn^{2+} and its ligating residues were imposed at Zn^{2+} -N (His) = 2.150 Å and Zn^{2+} -O (Asp) = 2.085 Å. Solvent content of these crystals was unusually high at 62.6%. Atomic coordinates of Zn-bound Pden1597 have been deposited in the PDB with entry code 4XRV. Figures were prepared using PyMol, which was also used for pairwise structural alignments of Pden1597 with other solute binding proteins.

RESULTS

Differential Expression of *pden1597* under Zn^{2+} and Mn^{2+} Starvation—The expression of *pden1597* and *pden4140* (a ZnuA homologue) were tested using qRT-PCR of *P. denitrificans* cells grown in Zn^{2+} -replete (50 μM added Zn^{2+}), Zn^{2+} -depleted (0 μM added Zn^{2+}), and Zn^{2+} -chelated (0 μM added Zn^{2+} , 50 μM TPEN) conditions. The third condition was chosen because ICP-OES of Zn^{2+} -depleted media showed a residual Zn^{2+} concentration of 350 nM, which is likely insufficient to induce conditions of extreme Zn^{2+} starvation (46). Consistent with this finding, growth curves for cells grown in Zn^{2+} -replete and Zn^{2+} -depleted conditions were virtually identical, whereas growth in the presence of TPEN was significantly inhibited (Fig. 2A). Zn^{2+} -depleted conditions gave rise to slight increases in expression levels for both genes relative to Zn^{2+} -replete conditions with increases in *pden1597* and *pden4140* expression of 1.4 ± 0.1 - and 2.0 ± 0.5 -fold, respectively (Fig. 2B). This effect was significantly enhanced in Zn^{2+} -chelated conditions, with expression levels of *pden1597* and *pden4140* increased by 4.8 ± 1.2 - and 23.3 ± 6.5 -fold, respectively, relative to Zn^{2+} -replete conditions. These results indicate that the expression of both *pden1597* and *pden4140* are enhanced under conditions of severe Zn^{2+} limitation.

To assess the metal specificity of the above effect, the expression levels of *pden1597* and *pden4140* were compared with those of *pden1259* (the putative Mn^{2+} transporter SBP) under conditions of Mn^{2+} limitation. Unlike Zn^{2+} , simple omission of Mn^{2+} from the culture medium resulted in a concentration of less than 40 nM by ICP-OES, sufficient to induce a relatively mild but significant growth defect in *P. denitrificans* (Fig. 2A). Under these conditions, neither *pden1597* nor *pden4140* were significantly up-regulated, whereas expression of *pden1259* increased by 5.6 ± 0.6 -fold relative to Mn^{2+} -replete conditions (Fig. 2C). These results suggested that like the ZnuA homo-

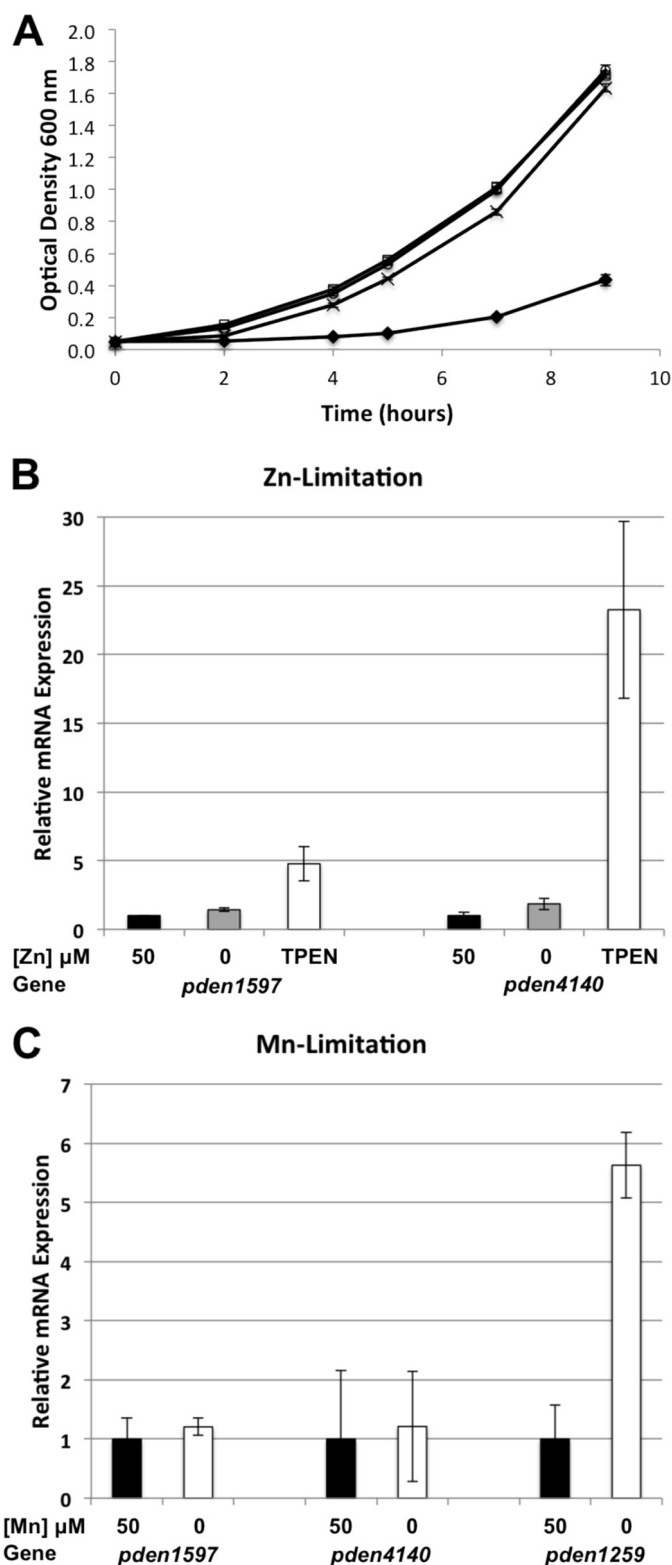


FIGURE 2. A, growth curves for *P. denitrificans* in metal-replete (open circles), Zn^{2+} -depleted (open squares), Mn^{2+} -depleted (crosses), and Zn^{2+} -chelated (filled diamonds) media. Data are the average of three independent biological replicates with error bars corresponding to the S.D. between replicates. B, relative expression levels of *pden1597* and *pden4140* under growth conditions containing 50 μM Zn^{2+} (black bars), 0 μM Zn^{2+} (gray bars), or 0 μM Zn^{2+} in the presence of 50 μM TPEN (white bars). Error bars represent the mean \pm S.E. ($n = 3$). C, relative expression levels of *pden1597*, *pden4140*, and *pden1259* under growth conditions containing 50 μM Mn^{2+} (black bars) and 0 μM Mn^{2+} (white bars).

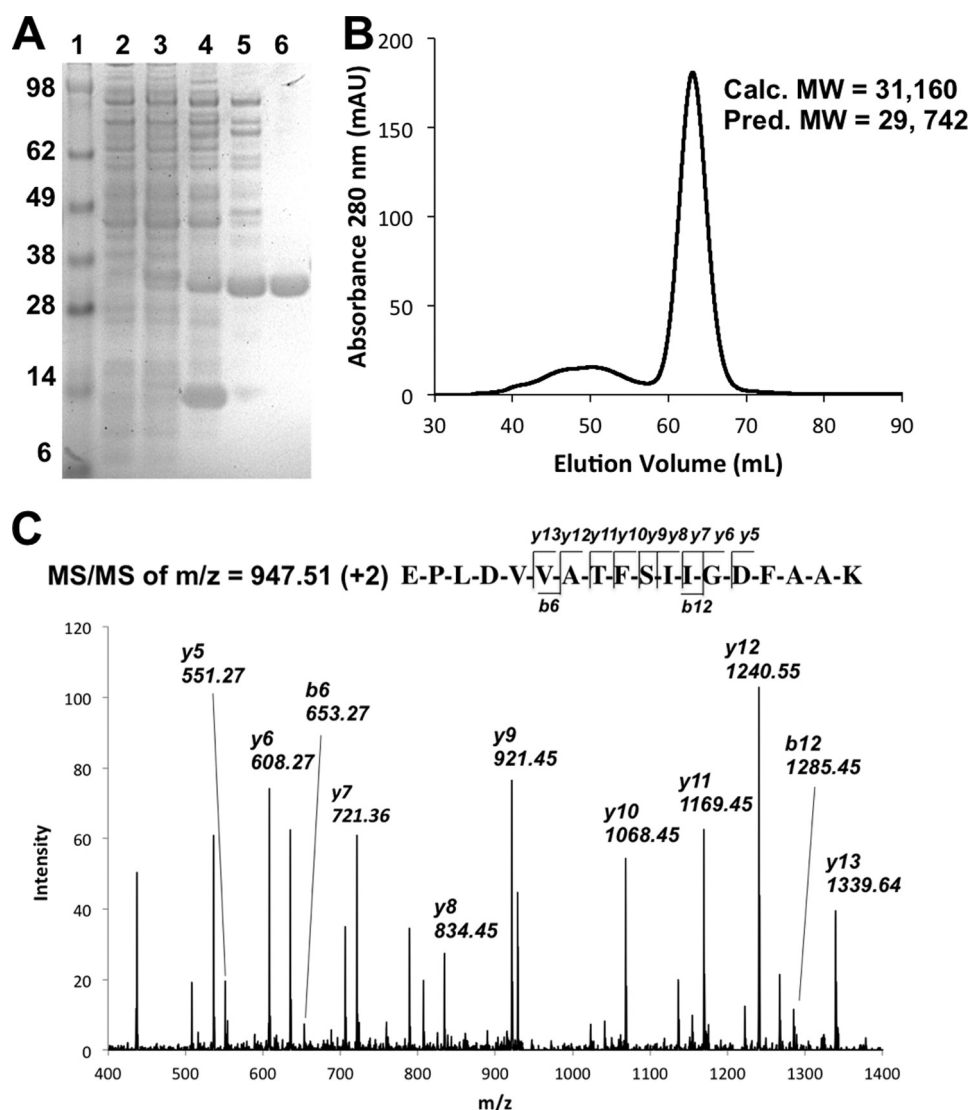


FIGURE 3. A, SDS-PAGE gel showing the purification of Pden1597. Lane 1, M_r ladder; lane 2, total cellular protein before isopropyl 1-thio- β -D-galactopyranoside induction; lane 3, total cellular protein after isopropyl 1-thio- β -D-galactopyranoside induction; lane 4, periplasmic fraction; lane 5, combined fractions containing Pden1597 after anion exchange chromatography; lane 6, combined fractions containing Pden1597 after size exclusion chromatography. B, size exclusion chromatogram showing purification of Pden1597 and the molecular weights calculated from the elution time (calc. MW) and the primary sequence (pred. MW). C, MS/MS spectrum of the 2^+ charge state of peptide Glu-25 to Lys-42. The monoisotopic $[M + 2H]^{2+}$ observed precursor m/z value was 947.01. The y- and b-ions identified are mapped onto the primary sequence.

logue *pden4140*, *pden1597* is a Zn^{2+} -specific transporter of the cluster 9 family of ABC transporters and prompted further studies on purified Pden1597 protein.

Expression and Purification of Pden1597—A plasmid bearing the full-length *pden1597* gene, including the N-terminal 22 residues comprising the predicted periplasmic localization signal peptide (47), was transformed into *E. coli* and overexpressed (Fig. 3A). SDS-PAGE identified a band of the correct size for full-length Pden1597 in the induced whole cell fraction, whereas a band of slightly smaller apparent M_r was enriched in the periplasmic fraction. This was subsequently identified by in-gel trypsin digest and mass spectrometry as Pden1597. A non-tryptic cleavage site between Ala-24 and Glu-25 was observed (Fig. 3C), indicating that the signal sequence is recognized by *E. coli* and cleaved upon export into the periplasm. The processed protein was purified to homogeneity from the periplasmic fraction by ion exchange and size exclusion chro-

matography (Fig. 3B). Size exclusion chromatography results further show that Pden1597 migrates exclusively as a monomer, with the molecular weight determined by elution time closely matching that calculated from primary sequence. Analysis of metal content by ICP-OES revealed that Pden1597 was isolated with nearly stoichiometric Zn^{2+} (0.95 equivalents) and undetectable levels of Mn^{2+} consistent with a specific role in Zn^{2+} import.

Metal Binding Affinities—Apo-Pden1597 was generated as described under “Experimental Procedures” and confirmed by ICP-OES to contain no more than 0.05 eq of Zn^{2+} . Careful optimization of the pH used during metal removal dialysis was required to prevent aggregation of the protein. Only preparations that ran as a single, monomeric peak during size exclusion chromatography were used for metal binding analysis. The chelating fluorophore MF-2 forms well characterized 1:1 complexes with transition metals and competition assays using this

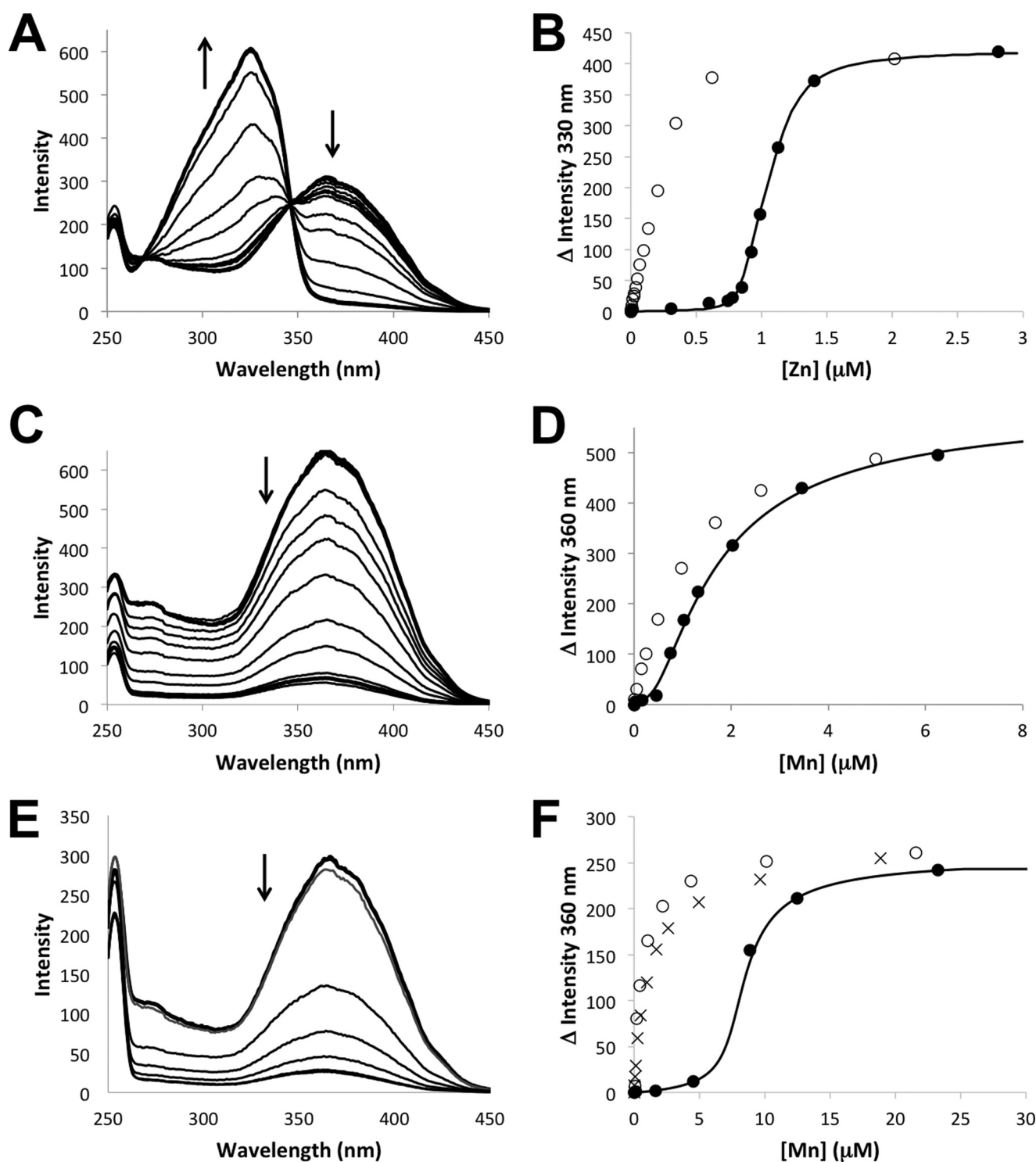


FIGURE 4. Representative fluorescence excitation spectra of a competition experiments between apo-Pden1597 and MF-2 titrated with Zn^{2+} (A) or Mn^{2+} (C and E). The initial and final spectra are shown as heavy lines and the direction of intensity changes with increasing metal are indicated by arrows. Changes in fluorescence intensity for MF-2 alone (open circles) or in the presence of apo-Pden1597 (filled circles) or Pden1597 as isolated (crosses) were plotted versus $[\text{Zn}]$ at 330 nm (B) or $[\text{Mn}]$ at 360 nm (D and F) and the competition data were fitted (solid line). The concentration of Pden1597 was 1.0 (A–D) or 15.0 μM (E and F). MF-2 was present at 0.4 (A, B, E, and F) or 0.8 μM (C and D).

molecule have been extensively used to estimate protein metal binding affinities (19, 30, 35, 48–51). The affinities of MF-2 for Mn^{2+} and Zn^{2+} have been determined at 0.97 μM and 36 nM, respectively, using competition assays against more weakly binding metals (35). These assays were reproduced to validate our experimental conditions, and essentially identical values

(K_d , Mn^{2+} = 0.97 μM ; K_d , Zn^{2+} = 33 nM) were obtained and used for fitting analyses.

Binding of Zn^{2+} to MF-2 causes a shift in the fluorescence excitation peak from ~ 360 to ~ 330 nm (Fig. 4A). Comparison of titrations of 0.4 μM MF-2 with Zn^{2+} in the presence and absence of 1.0 μM apo-Pden1597 (Fig. 4B) show that the protein

competes very effectively against MF-2 for Zn^{2+} binding, indicative of a significantly greater affinity. Using the determined K_d value of MF-2 for Zn^{2+} allowed us to calculate a K_d of Pden1597 for Zn^{2+} of 0.29 ± 0.13 nM and stoichiometry of $n = 0.94 \pm 0.19$ from three independent experiments.

Similar experiments were conducted with Mn^{2+} , which causes a quenching of fluorescence intensity (Fig. 4C). In this case, the presence of apo-Pden1597 has a more subtle, yet nonetheless, significant effect on the titration curve for MF-2 (Fig. 4D). This suggests that Pden1597 is also able to compete with MF-2 for Mn^{2+} . Indeed, fitting analysis yields a K_d of Pden1597 for Mn^{2+} of 52 ± 34 nM and $n = 0.54 \pm 0.03$ from three independent experiments. The reason for the low value of n is currently unclear. To confirm Mn^{2+} binding by Pden1597 in the presence of MF-2, we performed the experiment with an excess of apo-Pden1597 over MF-2 and obtained very similar results with $K_d = 35$ nM, $n = 0.52$ (Fig. 4, E and F). Finally, we repeated this experiment with 15 μM Pden1597 as isolated with nearly stoichiometric Zn^{2+} to assess whether Zn^{2+} and Mn^{2+} compete for the same binding site. The results show that Mn^{2+} does not bind to the protein as isolated, indicating that it cannot displace Zn^{2+} from its binding site. It is therefore evident that Pden1597 binds both Zn^{2+} and Mn^{2+} at the same site with high affinity, but binds Zn^{2+} with roughly 100-fold greater affinity, consistent with its likely role as a Zn^{2+} -specific transporter.

Holo- and Apo-protein Stability—Circular dichroism (CD) spectroscopy was used to observe the effect of Zn^{2+} and Mn^{2+} binding on the thermal stability of Pden1597 (Fig. 5). CD spectra for the apo-protein were virtually identical in the presence or absence of an excess of the relevant metal, indicating that metal binding does not result in any significant rearrangement of secondary structure (Fig. 5A). These samples were then subjected to increasing temperatures up to 90 °C, while monitoring the CD absorbance at 223 nm. The apo-protein exhibits a sharp transition and loss of ellipticity around $T_m = 63$ °C (Fig. 5B). The presence of Mn^{2+} had virtually no effect on melting temperature, increasing the T_m by no more than 2 °C. However, the Zn^{2+} -bound protein is remarkably stable, maintaining its CD spectrum up to 90 °C, indicating that the Zn^{2+} -bound form is by far the most stable form of Pden1597 studied. Regeneration of the native spectra after returning samples to 25 °C suggested that the loss of secondary structure was reversible in each case, although restoration of metal binding activity was not assessed.

Structure of Zn^{2+} -bound Pden1597—X-ray diffraction data of Pden1597 as purified from *E. coli* was collected and used to solve the crystal structure of Pden1597 to a final resolution of 2.72 Å (Table 1, Fig. 6). The overall structure is highly similar to those of other cluster 9 SBPs, with two structurally similar domains connected by a long α -helix. Two cysteine residues, Cys-158 and Cys-165 are positioned to form a disulfide bond and likely do so in the oxidizing environment of the periplasm. However, there is no electron density between the two sulfur atoms in the current structure, which is likely a result of radiation damage causing reduction of the disulfide bond (52).

The Zn^{2+} binding site consists of His-61 and His-138 from the N-terminal domain, and His-204 and Asp-279 from the C-terminal domain in a slightly distorted tetrahedral arrangement (Fig. 6, B and C) with average bond angles of $109 \pm 13^\circ$

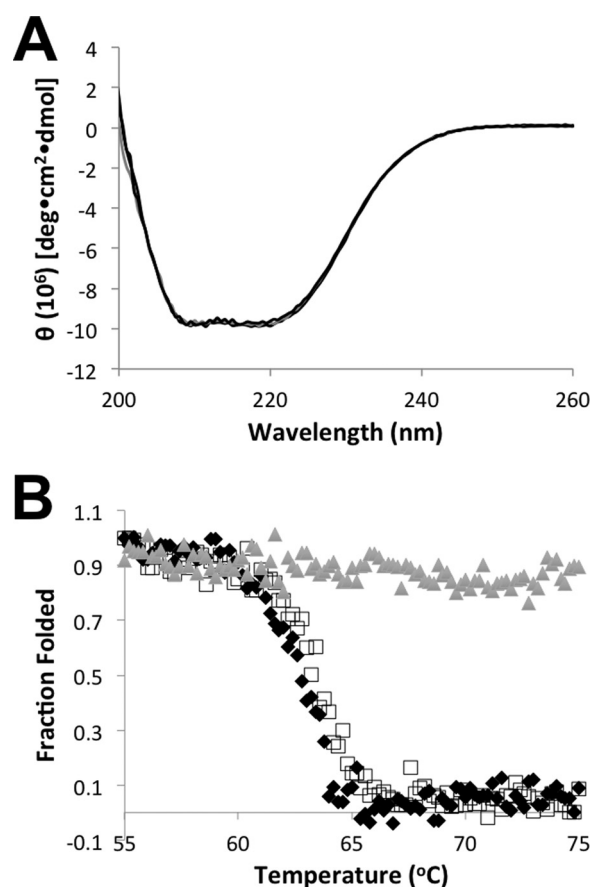


FIGURE 5. A, CD spectra of 15 μM apo-Pden1597 alone (solid black line) and in the presence of 40 μM Mn^{2+} (broken black line) and 40 μM Zn^{2+} (solid gray line). B, melt curve data measured at 223 nm for the samples in panel A, apo-Pden1597 alone (filled black diamonds), and in the presence of 40 μM Mn^{2+} (open black squares) and 40 μM Zn^{2+} (filled gray triangles).

TABLE 1
Data collection, processing, and refinement statistics

| | |
|---|------------------|
| Data collection | |
| Space group | C2 |
| Unit cell parameters | |
| <i>a</i> , <i>b</i> , <i>c</i> (Å) | 103.6 71.8 105.8 |
| α , β , γ (°) | 90.0 96.3 90.0 |
| Resolution range (Å) | 58.9–2.72 |
| Number of reflections (measured/unique) | 93,798/20,812 |
| R_{merge} | 0.12 (0.42) |
| $I/\sigma I$ | 5.9 (1.9) |
| Completeness (%) | 99.6 (100.0) |
| Redundancy | 4.5 (4.6) |
| Refinement statistics | |
| Resolution (Å) | 28.82–2.72 |
| $R_{\text{work}}/R_{\text{free}}$ | 21.0/26.7 |
| Number of atoms | |
| Protein | 3831 |
| Zn | 2 |
| Water | 18 |
| Other | 0 |
| R.m.s. deviations | |
| Bond lengths (Å) | 0.015 |
| Bond angles (°) | 2.08 |
| Average B-factor (Å ²) | 66.2 |

between the two independent metal sites in the asymmetric unit. Asp-279 is modeled as a monodentate ligand in Pden1597, as this preserves the tetrahedral symmetry of the complex and matches the coordination of the Glu ligand observed in other Zn^{2+} -specific SBP structures of higher resolution (18, 19). However, it should be noted that the resolution of the structure

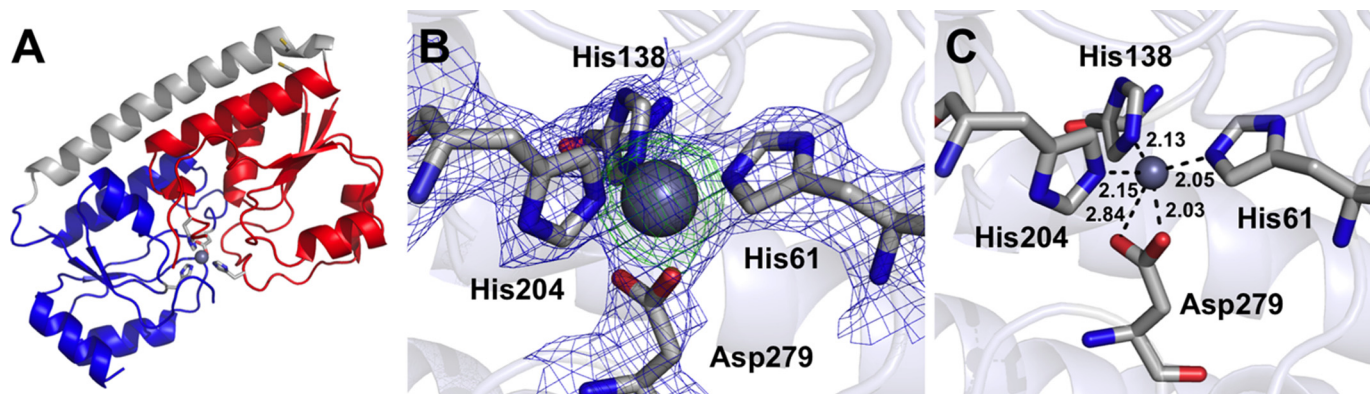


FIGURE 6. A, Overall structure of Pden1597 showing the N-terminal domain (blue), C-terminal domain (red), and connecting helix (gray) in schematic form. Metal ligands and Cys residues are shown in stick form colored according to atom type and the Zn^{2+} atom is shown as a gray sphere. B and C, the metal binding site of Pden1597. Blue electron density is for the $2F_o - F_c$ map of the refined structure and is contoured at 1.5σ . Green density is for the $F_o - F_c$ map of the structure omitting Zn^{2+} and is contoured at 5.0σ .

does not preclude the possibility of a bidentate arrangement. Similarly, the presence of a weakly bound water ligand cannot be absolutely ruled out. However, there is no electron density consistent with a water ligand, and its presence would disrupt the preferred 4-coordinate environment of the Zn^{2+} site (53). Second sphere hydrogen bonding interactions between the N δ atoms of His-138 and His-204 with the carboxylate oxygen atoms of conserved Asp-136 and Glu-253 are observed for Pden1597 as well as other cluster 9 SBPs and likely pre-organize the site for metal binding.

Residues 117–133 that comprise the abbreviated His-rich loop in Pden1597 are not resolved in the current structure (Fig. 7), nor has this loop been observed in any other structure of a Zn^{2+} -SBP to date. However, the loop may not be completely disordered in Pden1597. Significant electron density can be observed in this region, although it is insufficient to model with confidence at the current resolution. Nevertheless, it is clear that the relatively short His-rich loop of Pden1597 is positioned near the Zn^{2+} binding site and may play a role in Zn^{2+} acquisition or interaction with other ABC transporter components as has been suggested for other Zn-SBPs as discussed below.

DISCUSSION

The cluster 9 family of bacterial ABC transporters has been extensively studied due to its role in virulence (3). However, despite intense interest, the structural features mediating metal specificity and transport among this family remain imperfectly understood. We have chosen to study Pden1597 because it possesses attributes intermediate between Zn^{2+} -specific and Mn^{2+} -specific ABC transporters. To determine structural attributes critical for metal specificity in this protein, it was first essential to unambiguously assign that specificity. For this reason, we have determined the expression profiles for *pden1597* under conditions of Mn^{2+} and Zn^{2+} starvation as well as the *in vitro* binding affinities of the recombinant protein for these metals.

We have demonstrated using qRT-PCR that transcription of *pden1597* is sensitive to the availability of Zn^{2+} but not Mn^{2+} . This is likely due to the presence of a putative binding site for the Zn^{2+} -specific transcriptional regulator Zur in the promoter

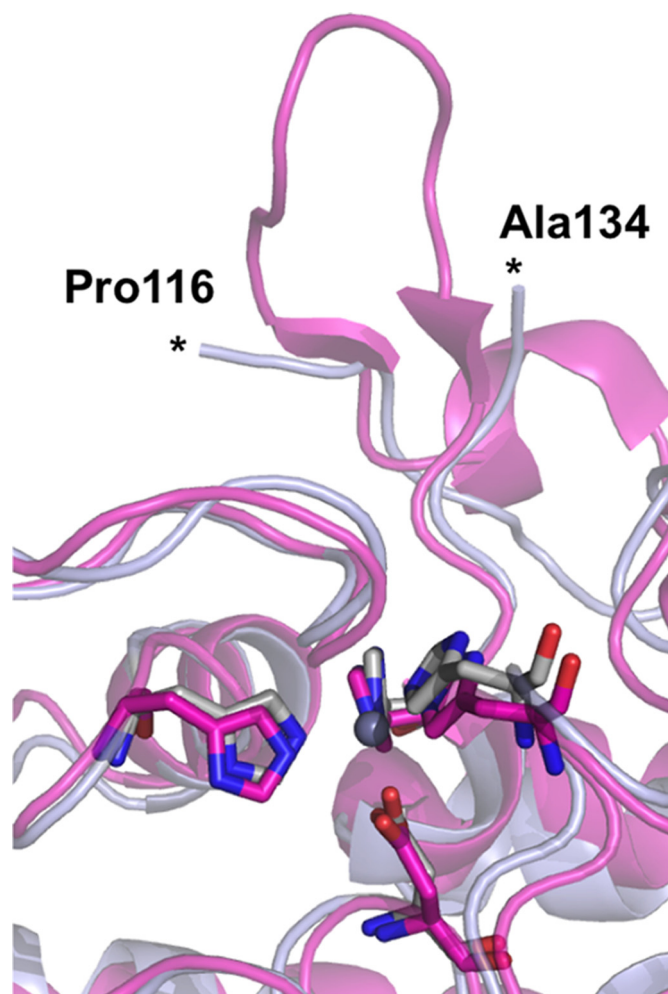


FIGURE 7. Overlay of the structures of Pden1597 (light blue) with that of Zn^{2+} -bound TroA (magenta, PDB accession 3MFQ) in schematic form with Zn^{2+} -binding residues shown in stick form colored according to atom type. Asterisks indicate the positions of residues beyond which the Pden1597 loop could not be modeled.

region of *pden1597* (54). We also determined dissociation constants for Pden1597 in the subnanomolar and low nanomolar ranges for Zn^{2+} and Mn^{2+} , respectively. This would suggest that Pden1597 could function as both a Zn^{2+} and Mn^{2+} carrier.

The ability to bind both metals at high affinity is shared by the homologues TroA (55), PsaA (24), and SitA (15). TroA and PsaA exhibit preferences for Mn^{2+} of ~ 3 - and ~ 70 -fold, respectively, whereas the binding affinities of SitA for these metals appear to be similar, although precise K_d values have not been determined. In the case of Pden1597, there is a >100 -fold preference for binding Zn^{2+} over Mn^{2+} . Combined with the sensitivity of *pden1597* transcription to Zn^{2+} but not Mn^{2+} availability, and the observation that recombinantly expressed Pden1597 contains Zn^{2+} exclusively, our data strongly suggests that Zn^{2+} is the physiologically relevant substrate for Pden1597.

CD spectra of Pden1597 are consistent with a predominantly α helical secondary structure that is essentially unchanged by Zn^{2+} or Mn^{2+} binding. However, the Zn^{2+} -bound form of Pden1597 was remarkably stabilized to thermal denaturation relative to the apo form, whereas Mn^{2+} binding had almost no effect. This trend has been observed for both Zn^{2+} - and Mn^{2+} -specific SBPs (19, 24, 55). In fact, imperfect coordination of Mn^{2+} relative to Zn^{2+} in PsaA leading to binding reversibility was shown to be essential for Mn^{2+} delivery to the membrane permease by PsaA (20). Thus, our CD results should not be taken as an indication of specificity. Rather, they show that Zn^{2+} binding to Pden1597 is very tight, with an essentially negligible off-rate. This in turn indicates that some conformational change accompanying binding to the membrane permease or other component of the ABC transporter system must be required for Zn^{2+} release.

It has been pointed out that specificity in the cluster 9 SBPs seems to depend upon three structural features (19). 1) A His at position 204 (Pden1597 numbering) indicates Zn^{2+} specificity, whereas a Glu at this position indicates Mn^{2+} specificity. 2) Coordination by Asp-279 indicates Mn^{2+} specificity. 3) The presence of a His-rich loop indicates Zn^{2+} specificity. To our knowledge, the structures of at least 10 different cluster 9 SBPs from various organisms have been determined by x-ray crystallography. Based on the above criteria, only the ZnuA homologues (14, 16–19) are predicted to be specific for Zn^{2+} , whereas the SitA (15), MntC (21, 22, 25), PsaA (20, 23, 24), and MtsA (26) homologues should be specific for Mn^{2+} . TroA is the only member of the group that violates these rules, having both His-205 (Zn-specific) and Asp-289 (Mn-specific) ligands and no His-rich loop (Mn-specific) (27–29). Although Mn^{2+} specificity has been demonstrated by *troA* knock-out studies in *S. suis* (56), it has a His₃, 1 carboxylate coordination sphere only observed thus far in Zn^{2+} -specific SBPs and binds Zn^{2+} with only slightly lower affinity than Mn^{2+} .

The role of coordination geometry in Zn^{2+} or Mn^{2+} specificity in the cluster IX SBP remains somewhat enigmatic. A relatively recent analysis of non-redundant metalloprotein crystal structures shows a strong preference of Zn^{2+} and Mn^{2+} for 4- and 6-coordinate environments, respectively (53). Pden1597 shares an identical tetrahedral coordination sphere with TroA (Fig. 7), yet has a roughly 100-fold greater affinity for Zn^{2+} over Mn^{2+} , whereas TroA has nearly equal affinities for both metals. Given that all TroA and Pden1597 structures are in complex with Zn^{2+} rather than Mn^{2+} , it is possible that the binding site is sufficiently flexible that the coordi-

nation sphere of Mn^{2+} in these proteins may differ from that of Zn^{2+} . However, structures of SitA (15) and PsaA (20) bound to both metals have been solved and show only very subtle changes in coordination. Indeed, non-ideal geometry around the Mn^{2+} ion in PsaA is thought to facilitate its release to the membrane permease, whereas the Mn^{2+} ion in SitA is in a nearly perfect octahedral geometry. Thus, it is clear that factors other than the coordination sphere have significant impacts on the specificity of metal binding and release in the cluster 9 family.

Pden1597 appears to have primary structural attributes consistent with both Mn^{2+} and Zn^{2+} specificity, including the presence of an abbreviated His-rich loop (Zn-specific) and coordination by Asp-279 (Mn-specific). To our knowledge, Pden1597 is the first SBP for a cluster 9 ABC transporter system that has confirmed specificity for Zn^{2+} , yet uses Asp-279 as a metal ligand. This would suggest that the most reliable determinant of Zn^{2+} specificity identifiable from the primary sequence alone is the presence of a His-rich loop near the metal binding site. This feature is proposed to be important in Zn^{2+} recruitment, mediating structural changes allowing metal transfer to the membrane permease, and/or Zn^{2+} sensing or scavenging from the periplasm (14, 17, 19, 57). Indeed, a second Zn^{2+} ion was identified bound to a His residue from the His-rich loop of *E. coli* ZnuA (19). However, we see no evidence for a second Zn^{2+} binding site in Pden1597. Therefore, the unstructured loop of Pden1597 may play a more significant role in the recognition of other components of the ABC transporter system than in metal acquisition.

The unstructured loop of Pden1597 is unusual not only for its brevity but also its sequence. There are relatively few His and Asp/Glu residues. Also, two Tyr residues are present that are not typically seen in these loop features. There are a few close homologues of Pden1597 with sequence identities greater than 50%, which include representatives from the human pathogens *Klebsiella pneumonia* and *Enterobacter aerogenes*. Among these, the sequence of the unstructured loop is well conserved and the residues of the metal binding site are absolutely conserved. None of these homologues have been characterized at any level to our knowledge, so it remains to be seen whether these will also be specific for Zn^{2+} binding. However, simply on the basis of sequence, Pden1597 and its homologues seem to form a subclass within the cluster 9 SBPs.

Here we have described the metal-dependent transcriptional regulation, metal binding properties, and structure of Pden1597, a previously uncharacterized SBP of the cluster 9 family of ABC transporters. On the basis of qRT-PCR results and the significant preference for Zn^{2+} binding over Mn^{2+} , we propose that the physiologically relevant metal for this ABC transporter system is Zn^{2+} . Due to the presence of a *znuABC* homologue in *P. denitrificans*, we suggest the name *aztABC* (auxiliary Zn^{2+} transporter) for the operon composed of *pden1595–1597*. Whether there are specific roles for the *znuABC* and *aztABC* operons in Zn^{2+} homeostasis or if they are simply redundant systems remains to be seen and experiments to determine this are currently underway in our laboratory.

Acknowledgments—We recognize Tanner Schaub at the Center for Animal Health, Food Safety and Bio-Security, New Mexico State University, for assistance with mass spectrometry and Tanis Hogg at Texas Tech University Health Sciences Center, El Paso, TX, for assistance in screening crystals. We further acknowledge the staff at the Berkeley Center for Structural Biology at Lawrence Berkeley National Laboratory for assistance at the beam line. Finally, we thank Dr. Carrie Wilmot, University of Minnesota, and Dr. Victor Davidson for critical reading of our manuscript. Final x-ray diffraction data was collected at the Berkeley Center for Structural Biology, which is supported in part by the National Institutes of Health, NIGMS, and the Howard Hughes Medical Institute. The Advanced Light Source is supported by the Director, Office of Science, Office of Basic Energy Sciences, of the United States Dept. of Energy under Contract DE-AC02-05CH11231.

REFERENCES

- Andreini, C., Bertini, I., Cavallaro, G., Holliday, G. L., and Thornton, J. M. (2008) Metal ions in biological catalysis: from enzyme databases to general principles. *J. Biol. Inorg. Chem.* **13**, 1205–1218
- Porcheron, G., Garénaux, A., Proulx, J., Sabri, M., and Dozois, C. M. (2013) Iron, copper, zinc, and manganese transport and regulation in pathogenic Enterobacteria: correlations between strains, site of infection and the relative importance of the different metal transport systems for virulence. *Front. Cell Infect. Microbiol.* **3**, 90
- Klein, J. S., and Lewinson, O. (2011) Bacterial ATP-driven transporters of transition metals: physiological roles, mechanisms of action, and roles in bacterial virulence. *Metalomics* **3**, 1098–1108
- Tam, R., and Saier, M. H., Jr. (1993) Structural, functional, and evolutionary relationships among extracellular solute-binding receptors of bacteria. *Microbiol. Rev.* **57**, 320–346
- Dintilhac, A., and Claverys, J. P. (1997) The *adc* locus, which affects competence for genetic transformation in *Streptococcus pneumoniae*, encodes an ABC transporter with a putative lipoprotein homologous to a family of streptococcal adhesins. *Res. Microbiol.* **148**, 119–131
- Claverys, J. P. (2001) A new family of high-affinity ABC manganese and zinc permeases. *Res. Microbiol.* **152**, 231–243
- Ammendola, S., Pasquali, P., Pistoia, C., Petrucci, P., Petrarca, P., Rotilio, G., and Battistoni, A. (2007) High-affinity Zn²⁺ uptake system ZnuABC is required for bacterial zinc homeostasis in intracellular environments and contributes to the virulence of *Salmonella enterica*. *Infect. Immun.* **75**, 5867–5876
- Bearden, S. W., and Perry, R. D. (1999) The Yfe system of *Yersinia pestis* transports iron and manganese and is required for full virulence of plague. *Mol. Microbiol.* **32**, 403–414
- Marra, A., Lawson, S., Asundi, J. S., Brigham, D., and Hromockyj, A. E. (2002) *In vivo* characterization of the *psa* genes from *Streptococcus pneumoniae* in multiple models of infection. *Microbiology* **148**, 1483–1491
- Gat, O., Mendelson, I., Chitlaru, T., Ariel, N., Altboum, Z., Levy, H., Weiss, S., Grosfeld, H., Cohen, S., and Shafferman, A. (2005) The solute-binding component of a putative Mn(II) ABC transporter (MntA) is a novel *Bacillus anthracis* virulence determinant. *Mol. Microbiol.* **58**, 533–551
- Clohesy, P. A., and Golden, B. E. (1995) Calprotectin-mediated zinc chelation as a biostatic mechanism in host defence. *Scand. J. Immunol.* **42**, 551–556
- Damo, S. M., Kehl-Fie, T. E., Sugitani, N., Holt, M. E., Rath, S., Murphy, W. J., Zhang, Y., Betz, C., Hench, L., Fritz, G., Skaar, E. P., and Chazin, W. J. (2013) Molecular basis for manganese sequestration by calprotectin and roles in the innate immune response to invading bacterial pathogens. *Proc. Natl. Acad. Sci. U.S.A.* **110**, 3841–3846
- Kehl-Fie, T. E., Zhang, Y., Moore, J. L., Farrand, A. J., Hood, M. I., Rath, S., Chazin, W. J., Caprioli, R. M., and Skaar, E. P. (2013) MntABC and MntH contribute to systemic *Staphylococcus aureus* infection by competing with calprotectin for nutrient manganese. *Infect. Immun.* **81**, 3395–3405
- Banerjee, S., Wei, B., Bhattacharyya-Pakrasi, M., Pakrasi, H. B., and Smith,

- T. J. (2003) Structural determinants of metal specificity in the zinc transport protein ZnuA from *synechocystis* 6803. *J. Mol. Biol.* **333**, 1061–1069
- Abate, F., Malito, E., Cozzi, R., Lo Surdo, P., Maione, D., and Bottomley, M. J. (2014) Apo, Zn²⁺-bound and Mn²⁺-bound structures reveal ligand-binding properties of SitA from the pathogen *Staphylococcus pseudintermedius*. *Biosci. Rep.* **34**, 743–758
- Chandra, B. R., Yogavel, M., and Sharma, A. (2007) Structural analysis of ABC-family periplasmic zinc binding protein provides new insights into mechanism of ligand uptake and release. *J. Mol. Biol.* **367**, 970–982
- Ilari, A., Alaleona, F., Petrarca, P., Battistoni, A., and Chiancone, E. (2011) The x-ray structure of the zinc transporter ZnuA from *Salmonella enterica* discloses a unique triad of zinc-coordinating histidines. *J. Mol. Biol.* **409**, 630–641
- Li, H., and Jøgl, G. (2007) Crystal structure of the zinc-binding transport protein ZnuA from *Escherichia coli* reveals an unexpected variation in metal coordination. *J. Mol. Biol.* **368**, 1358–1366
- Yatsunyk, L. A., Easton, J. A., Kim, L. R., Sugarbaker, S. A., Bennett, B., Breece, R. M., Vorontsov, I. I., Tierney, D. L., Crowder, M. W., and Rosenzweig, A. C. (2008) Structure and metal binding properties of ZnuA, a periplasmic zinc transporter from *Escherichia coli*. *J. Biol. Inorg. Chem.* **13**, 271–288
- Couñago, R. M., Ween, M. P., Begg, S. L., Bajaj, M., Zuegg, J., O'Mara, M. L., Cooper, M. A., McEwan, A. G., Paton, J. C., Kobe, B., and McDevitt, C. A. (2014) Imperfect coordination chemistry facilitates metal ion release in the Psa permease. *Nat. Chem. Biol.* **10**, 35–41
- Gribenko, A., Mosyak, L., Ghosh, S., Parris, K., Svenson, K., Moran, J., Chu, L., Li, S., Liu, T., Woods, V. L., Jr., Jansen, K. U., Green, B. A., Anderson, A. S., and Matsuka, Y. V. (2013) Three-dimensional structure and biophysical characterization of *Staphylococcus aureus* cell surface antigen-manganese transporter MntC. *J. Mol. Biol.* **425**, 3429–3445
- Kanteev, M., and Adir, N. (2013) Arginine 116 stabilizes the entrance to the metal ion-binding site of the MntC protein. *Acta Crystallogr. Sect. F Struct. Biol. Cryst. Commun.* **69**, 237–242
- Lawrence, M. C., Pilling, P. A., Epa, V. C., Berry, A. M., Ogunniyi, A. D., and Paton, J. C. (1998) The crystal structure of pneumococcal surface antigen PsaA reveals a metal-binding site and a novel structure for a putative ABC-type binding protein. *Structure* **6**, 1553–1561
- McDevitt, C. A., Ogunniyi, A. D., Valkov, E., Lawrence, M. C., Kobe, B., McEwan, A. G., and Paton, J. C. (2011) A molecular mechanism for bacterial susceptibility to zinc. *PLoS Pathog.* **7**, e1002357
- Rukhman, V., Anati, R., Melamed-Frank, M., and Adir, N. (2005) The MntC crystal structure suggests that import of Mn²⁺ in cyanobacteria is redox controlled. *J. Mol. Biol.* **348**, 961–969
- Sun, X., Baker, H. M., Ge, R., Sun, H., He, Q. Y., and Baker, E. N. (2009) Crystal structure and metal binding properties of the lipoprotein MtsA, responsible for iron transport in *Streptococcus pyogenes*. *Biochemistry* **48**, 6184–6190
- Lee, Y. H., Deka, R. K., Norgard, M. V., Radolf, J. D., and Hasemann, C. A. (1999) *Treponema pallidum* TroA is a periplasmic zinc-binding protein with a helical backbone. *Nat. Struct. Biol.* **6**, 628–633
- Lee, Y. H., Dorwart, M. R., Hazlett, K. R., Deka, R. K., Norgard, M. V., Radolf, J. D., and Hasemann, C. A. (2002) The crystal structure of Zn(II)-free *Treponema pallidum* TroA, a periplasmic metal-binding protein, reveals a closed conformation. *J. Bacteriol.* **184**, 2300–2304
- Zheng, B., Zhang, Q., Gao, J., Han, H., Li, M., Zhang, J., Qi, J., Yan, J., and Gao, G. F. (2011) Insight into the interaction of metal ions with TroA from *Streptococcus suis*. *PLoS One* **6**, e19510
- Graham, A. I., Hunt, S., Stokes, S. L., Bramall, N., Bunch, J., Cox, A. G., McLeod, C. W., and Poole, R. K. (2009) Severe zinc depletion of *Escherichia coli*: roles for high affinity zinc binding by ZinT, zinc transport and zinc-independent proteins. *J. Biol. Chem.* **284**, 18377–18389
- Wang, Y., Graichen, M. E., Liu, A., Pearson, A. R., Wilmot, C. M., and Davidson, V. L. (2003) MauG, a novel di-heme protein required for tryptophan tryptophylquinone biogenesis. *Biochemistry* **42**, 7318–7325
- Sullivan, M. J., Gates, A. J., Appia-Ayme, C., Rowley, G., and Richardson, D. J. (2013) Copper control of bacterial nitrous oxide emission and its impact on vitamin B12-dependent metabolism. *Proc. Natl. Acad. Sci. U.S.A.* **110**, 19926–19931

33. Edelhoch, H. (1967) Spectroscopic determination of tryptophan and tyrosine in proteins. *Biochemistry* **6**, 1948–1954
34. Shevchenko, A., Tomas, H., Havlis, J., Olsen, J. V., and Mann, M. (2006) In-gel digestion for mass spectrometric characterization of proteins and proteomes. *Nat. Protoc.* **1**, 2856–2860
35. Golynskiy, M. V., Gunderson, W. A., Hendrich, M. P., and Cohen, S. M. (2006) Metal binding studies and EPR spectroscopy of the manganese transport regulator MntR. *Biochemistry* **45**, 15359–15372
36. Kuzmic, P. (1996) Program DYNAFIT for the analysis of enzyme kinetic data: application to HIV proteinase. *Anal. Biochem.* **237**, 260–273
37. Kuzmic, P. (2009) DynaFit: a software package for enzymology. *Methods Enzymol.* **467**, 247–280
38. Dow, B. A., Tatulian, S. A., and Davidson, V. L. (2015) Use of the amicyanin signal sequence for efficient periplasmic expression in *E. coli* of a human antibody light chain variable domain. *Protein Expr. Purif.* **108**, 9–12
39. Luft, J. R., Collins, R. J., Fehrman, N. A., Lauricella, A. M., Veatch, C. K., and DeTitta, G. T. (2003) A deliberate approach to screening for initial crystallization conditions of biological macromolecules. *J. Struct. Biol.* **142**, 170–179
40. Battye, T. G., Kontogiannis, L., Johnson, O., Powell, H. R., and Leslie, A. G. (2011) iMOSFLM: a new graphical interface for diffraction-image processing with MOSFLM. *Acta Crystallogr. D Biol. Crystallogr.* **67**, 271–281
41. Winn, M. D., Ballard, C. C., Cowtan, K. D., Dodson, E. J., Emsley, P., Evans, P. R., Keegan, R. M., Krissinel, E. B., Leslie, A. G., McCoy, A., McNicholas, S. J., Murshudov, G. N., Pannu, N. S., Potterton, E. A., Powell, H. R., Read, R. J., Vagin, A., and Wilson, K. S. (2011) Overview of the CCP4 suite and current developments. *Acta Crystallogr. D Biol. Crystallogr.* **67**, 235–242
42. McCoy, A. J., Grosse-Kunstleve, R. W., Adams, P. D., Winn, M. D., Storoni, L. C., and Read, R. J. (2007) Phaser crystallographic software. *J. Appl. Crystallogr.* **40**, 658–674
43. Adams, P. D., Afonine, P. V., Bunkóczi, G., Chen, V. B., Echols, N., Headd, J. J., Hung, L. W., Jain, S., Kapral, G. J., Grosse Kunstleve, R. W., McCoy, A. J., Moriarty, N. W., Oeffner, R. D., Read, R. J., Richardson, D. C., Richardson, J. S., Terwilliger, T. C., and Zwart, P. H. (2011) The Phenix software for automated determination of macromolecular structures. *Methods* **55**, 94–106
44. Emsley, P., and Cowtan, K. (2004) Coot: model-building tools for molecular graphics. *Acta Crystallogr. D Biol. Crystallogr.* **60**, 2126–2132
45. Murshudov, G. N., Skubák, P., Lebedev, A. A., Pannu, N. S., Steiner, R. A., Nicholls, R. A., Winn, M. D., Long, F., and Vagin, A. A. (2011) REFMAC5 for the refinement of macromolecular crystal structures. *Acta Crystallogr. D Biol. Crystallogr.* **67**, 355–367
46. Outten, C. E., and O'Halloran, T. V. (2001) Femtomolar sensitivity of metalloregulatory proteins controlling zinc homeostasis. *Science* **292**, 2488–2492
47. Petersen, T. N., Brunak, S., von Heijne, G., and Nielsen, H. (2011) SignalP 4.0: discriminating signal peptides from transmembrane regions. *Nat. Methods* **8**, 785–786
48. de Seny, D., Heinz, U., Wommer, S., Kiefer, M., Meyer-Klaucke, W., Galleni, M., Frere, J. M., Bauer, R., and Adolph, H. W. (2001) Metal ion binding and coordination geometry for wild type and mutants of metallo- β -lactamase from *Bacillus cereus* 569/H/9 (BcII): a combined thermodynamic, kinetic, and spectroscopic approach. *J. Biol. Chem.* **276**, 45065–45078
49. Dutta, S. J., Liu, J., Hou, Z., and Mitra, B. (2006) Conserved aspartic acid 714 in transmembrane segment 8 of the ZntA subgroup of P1B-type ATPases is a metal-binding residue. *Biochemistry* **45**, 5923–5931
50. Liu, J., Dutta, S. J., Stemmler, A. J., and Mitra, B. (2006) Metal-binding affinity of the transmembrane site in ZntA: implications for metal selectivity. *Biochemistry* **45**, 763–772
51. Liu, J., Stemmler, A. J., Fatima, J., and Mitra, B. (2005) Metal-binding characteristics of the amino-terminal domain of ZntA: binding of lead is different compared to cadmium and zinc. *Biochemistry* **44**, 5159–5167
52. Burmeister, W. P. (2000) Structural changes in a cryo-cooled protein crystal owing to radiation damage. *Acta Crystallogr. D* **56**, 328–341
53. Dokmanić, I., Sikić, M., and Tomić, S. (2008) Metals in proteins: correlation between the metal-ion type, coordination number and the amino-acid residues involved in the coordination. *Acta Crystallogr. D Biol. Crystallogr.* **64**, 257–263
54. Shin, J. H., Oh, S. Y., Kim, S. J., and Roe, J. H. (2007) The zinc-responsive regulator Zur controls a zinc uptake system and some ribosomal proteins in *Streptomyces coelicolor* A3(2). *J. Bacteriol.* **189**, 4070–4077
55. Desrosiers, D. C., Sun, Y. C., Zaidi, A. A., Eggers, C. H., Cox, D. L., and Radolf, J. D. (2007) The general transition metal (Tro) and Zn^{2+} (Znu) transporters in *Treponema pallidum*: analysis of metal specificities and expression profiles. *Mol. Microbiol.* **65**, 137–152
56. Wichgers Schreur, P. J., Rebel, J. M., Smits, M. A., van Putten, J. P., and Smith, H. E. (2011) TroA of *Streptococcus suis* is required for manganese acquisition and full virulence. *J. Bacteriol.* **193**, 5073–5080
57. Wei, B., Randich, A. M., Bhattacharyya-Pakrasi, M., Pakrasi, H. B., and Smith, T. J. (2007) Possible regulatory role for the histidine-rich loop in the zinc transport protein, ZnuA. *Biochemistry* **46**, 8734–8743

**Transcriptional Regulation, Metal Binding Properties and Structure of Pden1597,
an Unusual Zinc Transport Protein from *Paracoccus denitrificans***

Melody Handali, Durga P. Neupane, Hridindu Roychowdhury and Erik T. Yukl

J. Biol. Chem. 2015, 290:11878-11889.

doi: 10.1074/jbc.M115.645853 originally published online March 18, 2015

Access the most updated version of this article at doi: [10.1074/jbc.M115.645853](https://doi.org/10.1074/jbc.M115.645853)

Alerts:

- [When this article is cited](#)
- [When a correction for this article is posted](#)

[Click here](#) to choose from all of JBC's e-mail alerts

This article cites 57 references, 11 of which can be accessed free at
<http://www.jbc.org/content/290/19/11878.full.html#ref-list-1>